*Desalination and Water Treatment*
www.deswater.com
doi: 10.5004/dwt.2020.26326

206 (2020) 273–285
December

# Selective chelation adsorption of copper ion on KH550 modified acid-activated attapulgite

Weiying Wang[a], Hongzhe Chen[b], Lin Wang[c], Shaogui Yang[d,*], Yong Wang[a,*]

[a]*State Environmental Protection Key Laboratory of Wetland Ecology and Vegetation Restoration, School of Environment, Northeast Normal University, Changchun, Jilin Province, China, Tel. +86-18628795197; email: wangy833@nenu.edu.cn (Y. Wang), Tel. +86-13578933513; email: wangwy808@nenu.edu.cn (W.Y. Wang)*
[b]*Ministry of Natural Resources, Third Institute of Oceanography, Xiamen, Fujian Province, China, Tel. +86-0592-2195219; email: chenhongzhe@tio.org.cn (H.Z. Chen)*
[c]*China Environment Publishing Group, Beijing, China, Tel. +86-010-67110245; email: wangalcn@126.com (L. Wang)*
[d]*School of Environment, Nanjing Normal University, Nanjing, Jiangsu Province, China, Tel. +86-25-85891849; Fax: +86-25-85891849; email: yangdlut@126.com (S.G. Yang)*

Received 2 August 2019; Accepted 16 July 2020

**ABSTRACT**

In this study, KH550 modified acid-activated attapulgites (KH550-HATP) were prepared and assessed for their capacity to remove Cu(II) ion from aqueous solution. The obtained adsorption behavior using different KH550-content KH550-HATP revealed that Cu(II) adsorption onto KH550-HATP followed pseudo-first-order kinetics and was mainly controlled by film diffusion mechanism. And there is a considerable contribution of the intraparticle diffusion effects for low KH550-content KH550-HATP. In addition, adsorption isotherms indicate that the adsorption pattern on KH550-HATP fit well with the Langmuir isotherm, and the maximum monolayer adsorption capacity for Cu(II) at temperatures of 283, 293, 303, and 313 K were 3.33, 5.92, 9.75, 13.85 mg $g^{-1}$, respectively, where the characteristic parameters for each adsorption isotherm were also determined. The adsorption process confirmed endothermic reactions in the range from 283 to 313 K. X-ray diffraction, X-ray photoelectron spectroscopy and Fourier-transform infrared spectroscopy patterns of KH550-HATP before and after Cu(II) adsorption manifest both interlayer ion exchange and surface complication play important roles. Results of competitive adsorption of several different metal ions show that KH550-HATP has adsorption capacity on $Cu^{2+}$, $Cd^{2+}$ and $Ca^{2+}$, among which $Cu^{2+}$ is chelated by KH550 selectively. These findings indicate that KH550-HATP could be an effective and environmentally friendly selective adsorbent for removing Cu(II) from wastewater.

*Keywords:* KH550 modified acid-activated attapulgites; Cu(II); Adsorption behavior; Adsorption mechanism

## 1. Introduction

Heavy metal contamination is a major environmental problem. Once leaching from landfill runoff [1], discharging from industrial/military wastewater [2] or erosion by acid rain [3], heavy metals may pose a threat to human health. In addition, heavy metals leaching into adjacent soil could reduce the complexity of soil bacteria [4]. In which, copper is an essential nutrient for humans, animals and

* Corresponding authors.

micro-organisms, but excess Cu(II) produces many toxic and harmful effects in living organisms [5]. Copper is mainly emanated from electroplating, electrical and metal finishing industries wastes. It is known to causes itching, gastrointestinal and possible changes in the liver and kidney, catarrh, Wilson disease, hypoglycemia and dyslexia [6].

There are a variety of treatment processes for heavy metal contaminated wastewater, including coagulation, hyperaccumulators, electrochemical process, membrane filtration and ion exchange/adsorption. Data obtained by neutron activation analysis revealed that ion exchange is one of the mechanisms underlying metal removal by the selected sawdust from the model solutions [7]. Adsorption process with benefits like simple operation and energy saving is a promising method in treating heavy metals. Kiruba et al. [8] used surface-modified eucalyptus seeds to remove Cu(II) ion from aqueous solutions by adsorption technology. Humic acid obtained from lignite waste can also have a good adsorption effect on $Cu^{2+}$ and $Pb^{2+}$ ions [9]. Nano-scale zero-valent iron impregnated cashew nut shells can also be used to remove copper ion [10]. In addition to creating no secondary pollution, adsorption with proper sorbents has been proved to be very effective in removing high toxicity pollutants at very low concentrations [11,12]. The key point is the selection of sorbents. There is growing interest in finding a sorbent with strong attractiveness and high selectivity. Sometimes, the selectivity of a sorbent is more important than its capacity, especially when dealing with micro-contamination. In recent decades, several types of adsorbents have been introduced into pollution control concerning heavy metals [13–20]. The feasibility of combining organic ligands with mesoporous silica to prepare nano-adsorbents to capture low levels of Pb(II) ions from aqueous solutions in batch systems was reported [21]. A sensitive and selective colorimetric method for simultaneous detection and removal of copper (Cu(II)) ion from contaminated water samples was developed based on the functional ligand embedded mesoporous conjugate materials [22]. Among all adsorbents, chemically stable and environment-friendly natural minerals are the preferred carrier in the natural water environment. Moreover, minerals like perlite [23] and manganese ore [24], have strong attractiveness to metal ions. Clay minerals with a negative charge are an important and potential low-cost adsorbent for the removal of metal ions, both for their high surface area and exchange capacities [25].

Attapulgite (ATP) and organically modified attapulgite composite had been used in copper ion adsorption [26]. However, most of these adsorbents lack selectivity without copper ion-imprinted functionalization [19]. The present study investigated the feasibility of using KH550 modified attapulgites for the selective adsorptive removal of copper ions. Using silane coupling agent KH550 instead of ion-imprinting reagents provides a variety of functional groups on attapulgites. Furthermore, KH550 is self-coupling to form a network on carrier [27] either by a covalent bond (Si–O–Si) or by a hydrogen bond between different molecules, which is more steady in complicated hydrological conditions. Spectroscopy methods like X-ray photoelectron spectroscopy (XPS) and Fourier-transform infrared spectroscopy (FTIR) were introduced here to discuss the adsorption mechanism. The study provides a new way of producing attapulgite adsorbent with copper ion selectivity.

## 2. Materials and methods

### 2.1. Materials

The natural attapulgite used in this work was purchased from Xuyi, Jiangsu of China. KH550 (Nanjing DebioChem Co., Ltd., China) was an analytical grade and used as received. Toluene and other chemicals (e.g., ethanol) used were of analytical grade. All solutions were prepared with twice-distilled water.

### 2.2. Material preparation

KH550 modified acid-activated attapulgite (KH550-HATP) was prepared by a modified method reported previously [28]. Acid treatment was conducted by placing 20 g of natural attapulgite in contact with 1 L of 2% nitric acid, and the suspension was constantly stirred for 48 h to remove carbonate and sorbed cations. The suspension was filtered and the residue was washed with distilled water until neutralization, dried at 383 K for 12 h and then manually ground to pass through a 200-mesh sieve. A certain quantity of HATP, 100 mL toluene and 8 mL KH550 were mixed in a 1 L flask and the mixture was dispersed with magnetic stirring (150 rpm) for 24 h. Then the suspension was filtered, washed 3 times, first with toluene and then with ethanol, washed with deionized water until neutralization, and then centrifuged. The residue was dried at 383 K for 12 h, and then manually ground to pass through a 200-mesh sieve.

### 2.3. Sorption experiments

#### 2.3.1. Batch experiment

The batch sorption experiments were conducted using 22 mL polytetrafluoroethylene vials at room temperature (298 K) except for the sorption thermodynamics test. 0.03 g of KH550-HATP was dispersed in 20 mL $Cu(NO_3)_2$ solution (initial pH 4.5), with the initial concentration of $Cu^{2+}$ in the range of 2.6 to 52.6 mg $L^{-1}$. The samples were kept in the dark and mixed end over end for 360 min. The residual concentration of $Cu^{2+}$ was determined by atomic absorption spectroscopy. All experiments were undertaken in triplicate and only mean value was presented.

The initial concentration of $Cu^{2+}$ was kept at 6.6 mg $L^{-1}$ in the following tests. The influence of sorbent mass on $Cu^{2+}$ sorption was studied with a sorbent dosage from 0.005 to 0.15 g. Ionic strength test was carried out by dispersing 0.03 g of sorbents in 20 mL salt solution (Table S1). The pH effect on $Cu^{2+}$ sorption was investigated in a pH range from 2 to 7, and the adsorption tests were performed at 283, 293, 303 and 313 K to study the effect of temperature. The solution pH was adjusted by adding 0.1 mol $L^{-1}$ of HCl or NaOH solutions.

In a competitive adsorption experiment at 298 K, the initial concentrations of metal ions including *M*1–*M*4 were listed in Table S1. The residual concentrations of metal ions were all determined by inductively coupled plasma atomic emission spectroscopy (ICP-AES). The other conditions were the same as those above.

#### 2.3.2. Sorption kinetic test

0.75 g of KH550-HATP was quickly introduced into a 500 mL three-neck flask with 500 mL of $Cu^{2+}$ solution (initial concentration 6.6 mg $L^{-1}$) during strong mechanical stirring. 2 mL of solution was withdrawn at different time intervals.

### 2.4. Material characterization

Zeta potentials of the samples were determined by a zeta potential analyzer (Brookhaven Instruments Corp., USA) according to Zhao et al. [29]. The concentrations of all samples in the zeta-potential analysis are kept at 1.5 g $L^{-1}$. Thermogravimetric analysis (TGA) was performed by the Pyris 1 TGA (PerkinElmer, Inc., USA) instrument. The weight of samples was about 2 mg, the heating rate was set at 20 K $min^{-1}$ in the range of 288–936 K. FTIR studies in the wave-number range of 400–4,000 $cm^{-1}$ were carried out in the transmission mode (Nicolet Co., Ltd., USA, NEXUS 870). XPS data were obtained with a PHI 5000 Versa Probe electron spectrometer from ULVAC-PHI using 300 W Al K$\alpha$ radiations. The base pressure was about $6.7 \times 10^{-8}$ Pa. The binding energies were referenced to the C 1s line at 284.6 eV from adventitious carbon, where the samples concerning KH550-HATP were referenced to the C 1s line at 285 eV from C–C or C–H bond. Brunauer–Emmett–Teller (BET) specific area of samples was determined by Micromeritics ASAP 2020 surface area and porosity analyzer. The crystalline phases of the samples were identified with an X-ray diffractometer with Cu KR radiation (Model, Shimadzu LabX XRD-6000).

### 2.5. Adsorption models

#### 2.5.1. Sorption isotherm

In a related experiment, 1 g $L^{-1}$ of KH550-HATP is added to avoid excess adsorption when dealing with a low concentration of copper ions. Langmuir model (Eq. (1)) assumes that adsorption occurs at a fixed number of localized sites on the surface, and all these sites are identical [30]. Adsorption of copper ions was evaluated using a separation factor $R_L$ defined as Eq. (2). The value of $R_L$ is always between 0 and 1. With $R_L$ considerably less than 1.0, the adsorption is considered to be favorable. $R_L = 0$ suggests the adsorption is irreversible [31]. On the other hand, the Freundlich model (Eq. (3)) is generally used to describe the adsorption isotherm on heterogeneous surfaces [32]. Temkin model (Eq. (4)) and Dubinin–Radushkevich (Eq. (5)) model are also applied.

$$\frac{C_e}{q_e} = \frac{1}{bq_{\max}} + \frac{C_e}{q_{\max}} \tag{1}$$

$$R_L = \frac{1}{1 + bC_0} \tag{2}$$

$$\log q_e = \log K_F + \frac{1}{n}\log C_e \tag{3}$$

$$q_e = \frac{RT}{B_t}\log k_t + \frac{RT}{B_t}\log C_e \tag{4}$$

$$\log q_e = \log q_D - B_D R^2 T^2 \log^2\left(1 + \frac{1}{C_e}\right) \tag{5}$$

$$E_a = \left(2P\right)^{-0.5} \tag{6}$$

where $q_e$ represents the amount of sorbed copper ion (mg $g^{-1}$), $C_0/C_e$ for initial/equilibrium concentration of a copper ion in solution (mg $L^{-1}$), $q_{\max}$ for the maximum monolayer sorption capacity (mg $g^{-1}$), and $b$ for the Langmuir sorption constant (L $mg^{-1}$, relating to the free energy of adsorption, reflecting the affinity of binding sites). $K_F$ is the Freundlich isotherm constant, $1/n$ (dimensionless) is the heterogeneity factor, as an indicator of adsorption intensity, $B_t$ (J $mol^{-1}$) and $k_t$ (L $mg^{-1}$) are Temkin isotherm parameters, $R$ is the gas constant (8.314 J $mol^{-1}$ $K^{-1}$), and $T$ is the absolute temperature (K). Concerning the Dubinin–Radushkevich model, each parameter should be expressed in standard units, where $B_D$ ($mol^2$ $kJ^{-2}$) is a constant related to the free energy of sorption as it migrates from the solution to the surface [33], and $q_D$ (mmol $g^{-1}$) is the Dubinin–Radushkevich isotherm constant, related to the adsorption capacity of the adsorbents [34]. Here, $RT \log(1 + 1/C_e)$ was Polanyi potential ($P$), and $E_a$ [26] can be calculated with Eq. (6). With the value of $E_a$ in the range of 1–8 kJ $mol^{-1}$ indicating physical adsorption [35], whereas the value between 8 and 16 kJ $mol^{-1}$ reveals an ion-exchange process [26]. The values of the linear correlation coefficients were also calculated and provided.

#### 2.5.2. Kinetics models

Pseudo-first-order (or quasi-first-order) kinetic model assumes that in a reaction with a second-order reaction rate incorporating two reactants (adsorbent and adsorbate), one of the reactants (adsorbent) concentrations remains constant as the reaction proceeds. The concentration of adsorbate involved actually at time $t$ is $C_t$, quasi-first-order equation describes an adsorptive process with limited adsorbates and adequate adsorptive sites as follows:

$$C_t = C_{e1}\left(1 - e^{-k_1 t}\right) \tag{7}$$

where $k_1$ is the rate constant of pseudo-first-order adsorption (L $min^{-1}$), $C_t$ is the concentration of adsorbate at $t$, and $C_{e1}$ is the equilibrium concentration of pseudo-first-order adsorption (mg $L^{-1}$).

Pseudo-second-order (or quasi-second-order) kinetics model where chemical adsorption involving valent forces between adsorptive sites and divalent metal ions is viewed as the rate-limiting step [36]. Therefore, the rate expression is given as $C_t = \frac{k_2 t C_{e2}^2}{1 + k_2 t C_{e2}}$, but since the values of $1/C_{e2}$ are overdispersed for linear fitting, the equation can also perform as:

$$\frac{1}{C_t} = \frac{1}{k_2 t C_{e2}} + \frac{1}{C_{e2}} \tag{8}$$

where $k_2$ is the rate constant of pseudo-second-order adsorption (L $min^{-1}$), and $C_{e2}$ is the equilibrium concentration of pseudo-second-order adsorption (mg $L^{-1}$).

Elovich kinetic equation [37] is a rate equation for chemisorption concerning a few reaction mechanisms including bulk/surface diffusion and activation/deactivation, given as follows:

$$q_t = \frac{1}{\beta}\ln(\alpha\beta) + \frac{1}{\beta}\ln(t) \quad (9)$$

where $\alpha$ is the initial adsorption rate (mg g$^{-1}$ min$^{-1}$) and $\beta$ is the desorption constant (g mg$^{-1}$).

Adsorption is a multi-step process involving adsorbate transport from aqueous phase onto the surface (film diffusion), then followed by adsorbate diffusion into intraparticle pores (intraparticle diffusion). The intraparticle diffusion is expressed by the following equation [37]:

$$q_t = k_3 t^{0.5} + C \quad (10)$$

where $C$ is the intercept and $k_3$ is the intraparticle diffusion rate constant. To determine the actual process involved, another equation can be applied. $B_t$ is defined as a calculated mathematical function as follows:

$$B_t = -\ln(1 - F) - 0.4799 \quad (11)$$

where $F_t$ is the fractional attainment of equilibrium at time $t$, and $F_t = q_t/q_e$. $B_t$ values were then plotted against $t$. If the plot is a line passing through the origin, the relating behavior is governed by the intraparticle diffusion mechanism, otherwise, it is governed by the film diffusion process [26].

## 3. Results and discussion

### 3.1. Characterization

X-ray diffraction (XRD) patterns of KH550-HATP were provided in Fig. S1. The $d_{001}$ spacing of ATP/HATP calculated by using the Bragg equation is 1.055 nm, and that of KH550-HATP is 1.06 nm with a negligible small peak arising at 4.46° (2θ), which accounts for 1.98 nm of $d_{001}$ spacing. It seems that most of KH550 is a coating on the surface of HATP instead of intercalation. After acidic treatment, the peak at 10.12° disappears, which could be explained by the exchange of $Na^+$ by $H^+$ [38]. After adsorption of copper ions, the intensity of the peak at about 8° is significantly reduced. When at 8°, the peak shapes of ATP and copper adsorbed KH550-HATP are almost the same, it might be attributed to the exchange of $H^+$ by $Cu^{2+}$ during copper ion adsorption; this confirms the role of interlayer ion-exchange process on KH550-HATP during copper adsorption, which cannot be ignored.

The silane coupling agent can form Si–O–M on the carrier, and the binding energy of Si–O is larger than that of C–O, which is more stable for application. *M* represents Mg, Al or Si concerning HATP. The investigation in surface elements by XPS spectra shows both Mg/Si (0.13) and Al/Si (0.24) are less than 0.25 on HATP, so the most possible binding is Si–O–Si. The percentage weight change of the samples vs. temperature was evaluated and shown in Fig. S2. All the samples undergo water molecular evaporation at 300–400 K and lead to a rapid decrease in weight. Then the weight of ATP and KH550-HATP decreases to 86% with the temperature increasing, whereas the weight of HATP decreases at a much slower rate. This may be attributed to the mineralization of organic carbon or other impurities in ATP, which has been removed by the acid-activation process in HATP. Obviously, when the temperature is higher than the impurities (600–700 K), the strong binding of the silane coupling agent on KH550-HATP would be removed. The weight loss also reflects the actual loading amount of KH550 on KH550-HATP indirectly.

BET specific surface areas of ATP, HATP and KH550-HATP are 163.04, 173.77 and 127.59 m$^2$ g$^{-1}$, respectively. While acid-activation enlarges the surface area of ATP, the silane coupling agent greatly reduces this surface area. Therefore, the specific surface area is not the most important factor affecting the adsorption effect in this study.

Zeta potentials of ATP, HATP and KH550-HATP as a function of solution pH in the range from 1 to 7 are shown in Fig. 1. Since the surface charge of the sorbents is affected by solution pH, the negative zeta potentials when solution pH > 2 indicate that both ATP and HATP have permanently negative charges on their surfaces. It also illustrates their pH values at the point of zero charge ($pH_{zpc}$) are below 2.0 (~1.2 for ATP). HATP has more negative charges than ATP as a result of the decrease in molar mass of material and the increase in negatively charged groups (e.g., Si–OH) in the acidification process [39]. Compared with that on HATP, it seems that negative charges on KH550-HATP decrease. These may be ascribed to the protonation of amino groups on KH550-HATP. In addition, negatively charged groups on HATP can react with Si–O of KH550 introduced by esterification reaction and be removed. The $pH_{zpc}$ is estimated to be about 3.8 for KH550-HATP.

FTIR patterns are provided in Fig. 2. 950–1,250 cm$^{-1}$ region can be attributed to asymmetric T–O stretching mode [40]. 1,014 cm$^{-1}$ stands for Si–O stretching vibration when 509 cm$^{-1}$ corresponds to Si–O asymmetrical bending vibrations. In addition to Si–O band, there are several bands present in all four samples, and other bands appear in KH550-HATP or copper ion adsorbed samples. For example, the peaks at around 3,417 and 1,648 cm$^{-1}$ are assigned to the

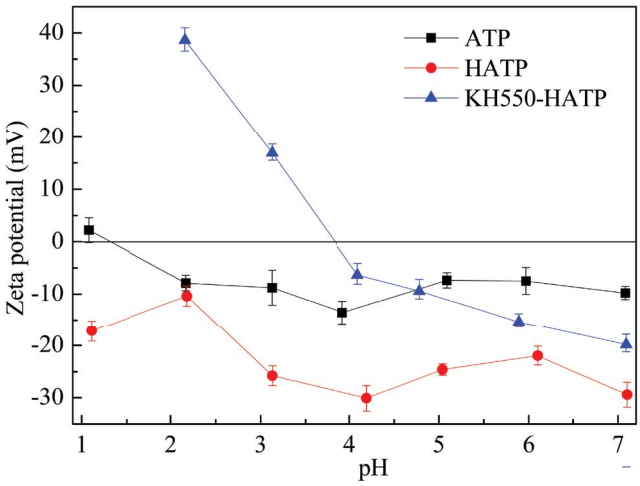


Fig. 1. Zeta potentials at different pH for three types of material: ATP, HATP and KH550-HATP.

stretching vibration and bending vibration of O–H groups in all samples, respectively, whereas the peaks at 3,253 and 3,066 $cm^{-1}$ for N–H stretching vibration, at 2,850 and 2,933 $cm^{-1}$ for aliphatic C–H stretching vibration of $CH_2R_2$ group, at 1,508 $cm^{-1}$ for N–H bending vibration, at 1,471 $cm^{-1}$ for C–H bending vibration of $CH_3$ group, at 1,448 $cm^{-1}$ for aliphatic C–H bending vibration of $CH_2R_2$ group and at 1,415 $cm^{-1}$ for C–N stretching vibration is only found on KH550-HATP and adsorbed samples. The peak at 1,380–1,520 $cm^{-1}$ on the ATP curve might be from C–C or other bonds from impurities and removed by acid-treatment. The sharp peak at 1,380 $cm^{-1}$ on KH550-HATP after copper ion adsorption should be ascribed to N–O of $NO_3^-$. The peak at 426 $cm^{-1}$ is assigned to the bending vibration of O–Si–O, and the new peak at 418 $cm^{-1}$ should be from O–Si–O by the binding of the silane coupling agent. Thus the results obtained from FTIR studies indicate that the ATP and modified material all have a variety of functional groups that may be contributing to the adsorption of Cu(II) ions. Copper ion is a soft acid ion with a small hydration radius. Low dehydration barrier makes it easy for direct complexation of a copper ion with amino groups (with lone pair electrons) on KH550 in aqueous solution. After copper ion adsorption, new sharp peaks arise because of chelation adsorption of copper ion (Fig. 3). 434 and 443 $cm^{-1}$ appear for stretching vibration of Cu–O($H_2O$/–OH) and Cu–N(–$NH_2$). The peak of Si–O deformation vibration shifts from 467 to 459 $cm^{-1}$ after adsorption. Since an amino group is found on the surface of KH550-HATP, it is inferred that the functional group acting is an amino group.

### 3.2. Effect of initial pH

The effect of pH on copper ion adsorption capacity of HATP and KH550-HATP was investigated. $H^+$ could compete with $Cu^{2+}$ in the adsorption process, so lower pH in solution leads to lower adsorption capacity in both samples (Fig. S3) [41,42]. In addition, the copper ion adsorption capacity of KH550-HATP is obviously higher than that of HATP in the pH values exceed 4. For example, the copper ion adsorption capacity of KH550-HATP and HATP in pH 4 are 4.17 and 2.83 mg $g^{-1}$, respectively. Note that the specific surface area of KH550-HATP (127.59 $m^2$ $g^{-1}$) is much lower than that of HATP (173.77 $m^2$ $g^{-1}$), which confirms the non-selective physisorption process could not be ascribed to the enhanced adsorption of $Cu^{2+}$ on KH550-HATP for its porous morphology. Because the chelating adsorption of copper ion onto KH550 is supposed to be a surface process (Fig. 3), it provides active adsorption sites in addition to inner sites, the same as HATP. However, with a pH value lower than 3, the adsorption capacities of HATP and KH550-HATP are almost the same, because of the protonation of amino groups on KH550-HATP. Positively charged sites (–$NH_3^+$) stop copper ion from approaching. Meanwhile, since protonated amino groups lose a lone pair of electrons, copper ion could not be adsorbed onto these sites by the chelation process.

### 3.3. Kinetic studies

The effect of four different KH550 content of KH550-HATP on copper ion adsorption was investigated. The samples were renamed as *K–X*, where *X* represented the volume ratio of toluene and KH550. The fitting parameters calculated by these non-linear equations are listed in Table S2.

As seen from Fig. 4, the sorption of copper ion onto K-100/8 is fast at the beginning of the experiment (0–90 min) and slower from 90 to 180 min, and finally reaches a plateau after 180 min. Generally speaking, higher contents of KH550 brings higher rate constant, though K-100/10 is the exception, which implies the dispersion of KH550 coating on HATP is also an important factor affecting the adsorption of copper ion. The plots for all KH550 contents follow well with the quasi-first-order kinetics model (Table S2). And linear regression values ($R^2$) of quasi-second-order kinetics model increase with rising KH550 contents, indicating valent forces between KH550 and divalent copper ion can be dominant on high-KH550-content material. Conversely, low-content materials follow well Elovich kinetics model. Note that the Elovich model has been broadly applied to describe the kinetics of sorption and desorption of inorganic

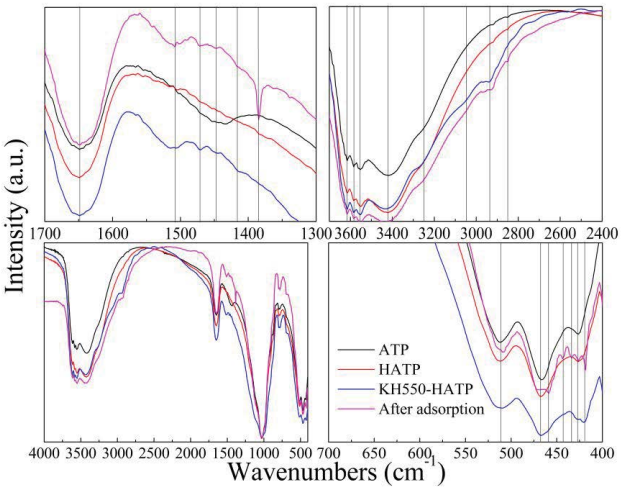


Fig. 2. FTIR patterns for three types of material: ATP, HATP and KH550-HATP. In that KH550-HATP after copper ion adsorption process is also provided.

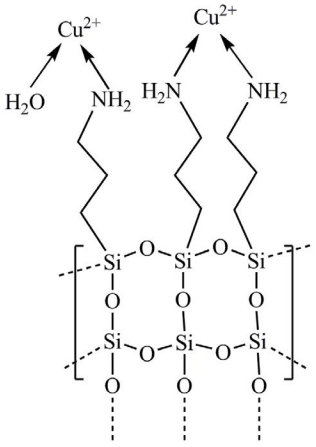


Fig. 3. The proposed surface chelation mechanism of $Cu^{2+}$ onto KH550-HATP.

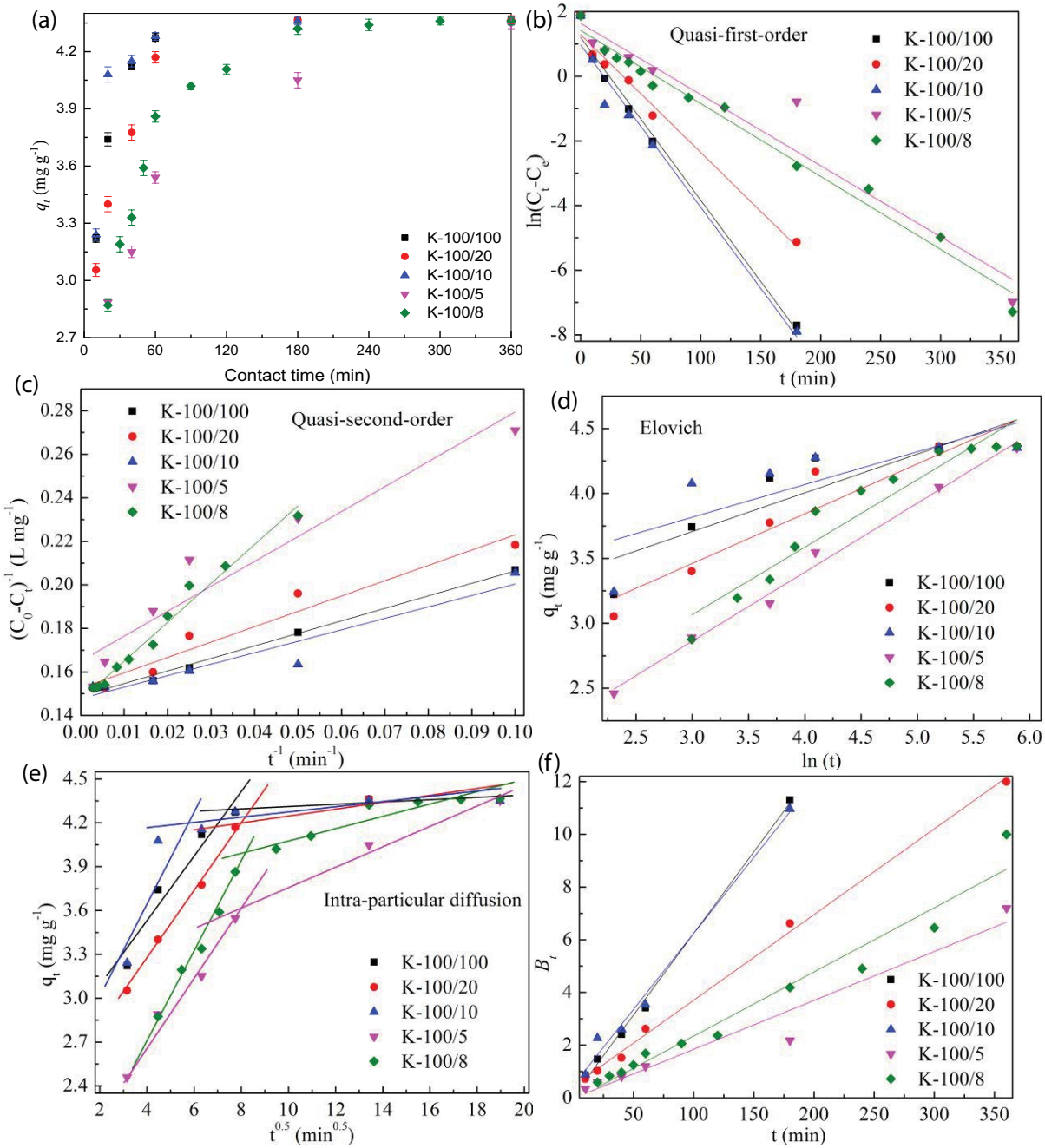


Fig. 4. Sorption kinetics of copper ion onto KH550-HATP. (a) Sorption kinetics experimental date, (b) Quasi-first-order model, (c) Quasi-second-order model, (d) Elovich model, (e) intraparticular diffusion model, and (f) $B_t$ vs. $t$ plot.

on soil [43], copper ion adsorption and desorption on HATP with lower KH550-content would be more important, where ion exchange is the dominant process. In all, the mechanisms of copper ion on KH550 and HATP are quite different.

From the intraparticle diffusion model (Fig. S3), there is a two-step adsorption process (film diffusion and gradual adsorption with film diffusion and intraparticle diffusion operating simultaneously). Since the plot of $q_t$ vs. $t^{0.5}$ does not pass through the origin, intraparticle diffusion is not the only rate-controlling step [44], instead, the low $R^2$ of intraparticle diffusion model indicates that surface adsorption might be the rate-limiting step (Table S2), especially for the high-KH550-content material. The same conclusion could be drawn from $B_t$ vs. $t$ plot. The intercepts of lines for high-KH550-content materials are much larger than low-content ones, indicating that adsorption processes for high-KH550-content materials are governed by film diffusion. Note that K100/100 with the highest contents of KH550 provides almost the lowest $R^2$ value; it seems the presence of KH550 is the reason of surface-controlled process, while the intraparticle diffusion is more important in copper ion adsorption process onto HATP. In other words, the higher

the proportion of KH550, the less the membrane diffusion and intraparticle diffusion are restricted, and the stronger the adsorption capacity of copper ions. Therefore, considering the combined adsorption of copper ions by KH550 and HATP, the volume ratio of toluene and KH550 is set to 100/8 as the best condition.

### 3.4. Adsorption isotherms of copper ion on KH550-HATP and adsorption thermodynamics

Adsorption isotherms at different temperatures are presented in Fig. 5. The two most commonly employed models are the Langmuir and Freundlich isotherms. The linear Langmuir/Freundlich adsorption isotherms of KH550-HATP at 283, 293, 303 and 313 K are illustrated in Fig. S4. The Langmuir/Freundlich parameters and correlation coefficients ($R^2$) are calculated from the slope and intercept of the graphs (Table S3). The maximum monolayer adsorption capacity for Cu(II) at temperatures of 283, 293, 303, and 313 K were 3.33, 5.92, 9.75, 13.85 mg $g^{-1}$, respectively. These values are higher than that of fresh/composted swine manure [45] with adsorption capacity less than 10 mg $g^{-1}$. At higher temperatures (303 and 313 K), adsorption isotherms of KH550-HATP better follow Langmuir equation, whereas those at low temperatures follow well both Langmuir equation and Freundlich equation (Fig. 5 and Table S3). Considering that the Langmuir model is supposed to preferably describe the coordination mechanism-led adsorption process [46,47], while Freundlich model fits the ion-exchange process better [46,48], it could be inferred that coordination process by KH550 became more important with a temperature rising. $R_L$ values in 303 and 313 K are much lower than those in the presence of chitosan [49] even with lower $C_0$ concerned, indicating that KH550 is a more appropriate chelation adsorbent than chitosan at 303–313 K. In other words, the optimal temperature for KH550-HTAP to adsorb copper ions should be 313 K.

Usually, both coordination and ion-exchange adsorption processes in aqueous solution are endothermic [46,48,49], consistent with this work, so these results also imply that endothermic features of coordination mechanism are more obvious. Additionally, at higher temperatures like 303 or 313 K, a small decrease in $q_e$ can be found at high $C_e$ value, principally because of disruption from coordination between copper ions and nitrate ions at high temperatures with a high concentration of copper nitrate. Temkin equation and Dubinin–Radushkevich equation was also employed herein. $R^2$ indicates that the experimental data also fit well to the Temkin equation and Dubinin–Radushkevich equation, but $R^2$ of both equations are lower than those of Langmuir equation at high temperature and those of Freundlich equation at low temperature. All of $E_a$ values except that at 313 K are around 16 with $R^2 > 0.9$, implying that neither the effect of ion exchange nor that of coordination can be ignored in the adsorption process at relatively low temperature. According to thermodynamic analysis, these results also show that the adsorption of copper ions by KH550-HATP is a coordination and ion exchange process and an endothermic process.

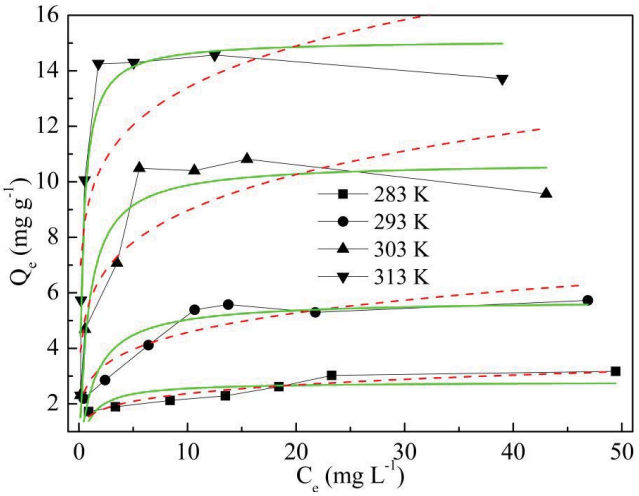


Fig. 5. The adsorption isotherms of $Cu^{2+}$ by KH550-HATP at different temperatures (283, 293, 303 and 313 K): Freundlich (red dash), Langmuir (green solid).

### 3.5. Competitive adsorption and the mechanism

Competitive adsorption of different metal ions was investigated. In *M*4 (mixture solution 4), only the concentrations of $Cu^{2+}$, $Cd^{2+}$ and $Ca^{2+}$ decrease obviously (Table 1), indicating that KH550-HATP has adsorption capacity for $Cu^{2+}$, $Cd^{2+}$ and $Ca^{2+}$. Meanwhile, the saturation adsorption capacities of $Cu^{2+}$ are basically neither disrupted by $Cd^{2+}$ and $Ca^{2+}$ sorption, nor by other metal ions (Table 2), which implies that the main adsorption sites of $Cu^{2+}$ might be different from that of $Cd^{2+}$ and $Ca^{2+}$. Gao et al. [50] suggested that amidoxime group had a share in coordination with heavy metal ions, where he believed the adsorption capacity is in the order of $Cu^{2+} >> Ni^{2+} > Pb^{2+} > Cd^{2+}$. Im et al. [51] proposed the selective adsorption of copper ion in $Cu^{2+}$, $Cd^{2+}$ and $Zn^{2+}$ mixture solution by amino-group. But current research on KH550-HATP is different. Though only amino-group can be found on the surface of KH550-HATP, $Cd^{2+}$ adsorption is negligible, the same as that of $Ca^{2+}$. It can be inferred that in the presence of a high concentration of $Cu^{2+}$, due to the preferential coordination of $Cu^{2+}$, the main reason for removing $Cd^{2+}$/$Ca^{2+}$ from the aqueous solution is not the complexation of the inner sphere with the amino group.

Table 1
Competitive adsorption experiment of KH550-HATP in mixture solution 4 (*M*4)

| Concentration (mg $L^{-1}$) | Initial concentration | Rest concentration |
|---|---|---|
| $Cu^{2+}$ | 26.3 | 15.47 |
| $Ca^{2+}$ | 26.3 | 14.56 |
| $Cd^{2+}$ | 26.3 | 13.16 |
| $Co^{2+}$ | 26.3 | 26.11 |
| $Mg^{2+}$ | 26.3 | 25.06 |
| $Ni^{2+}$ | 26.3 | 26.6 |
| $Na^{+}$ | 26.3 | 26.46 |
| $K^{+}$ | 26.3 | 24.43 |

Table 2
The impact of different ions on the adsorption of copper ion

| Different solution | $q_e$ for $Cu^{2+}$ | Control group[a] ($q_e$) |
|---|---|---|
| *M*1 | 4.34 | 4.36 |
| *M*2 | 4.02 | 4.05 |
| *M*3 | 3.99 | 4.05 |
| Cd | 4.34 | 4.36 |
| Mg | 4.34 | 4.36 |
| Ni | 4.34 | 4.36 |
| Na | 4.33 | 4.36 |
| K | 4.33 | 4.36 |
| Ca | 4.34 | 4.36 |
| Co | 4.34 | 4.36 |

[a]6.6 mg $L^{-1}$ of a copper solution except for *M*2 and *M*3.

The XPS peak of Si 2P spectra (Fig. 6) moves to the high-energy side. The decrease in the outer electron density of Si leads to the weakened shielding effect. The relative enhancement of the Coulomb force between the inner-shell electron and the atomic nucleus should be corresponding to binding energy increasing in Si. It might be due to the adsorption of $Ca^{2+}$/$Cd^{2+}$/$Cu^{2+}$ on Si–$O^-$/Si–OH by internal coordination or static electricity. This result indicates that some of the divalent heavy metals could be adsorbed directly on oxygen attached to silicon.

After adsorption, a slight peak displacement (–0.5 eV) on the N 1s peak could be observed (Fig. 7). N 1s peak at 402.2 eV is corresponding to protonated amino-group of KH550, because of the chelation of copper ion on amino-group. This verifies the enhancement of copper ion adsorption on KH550-HATP, which is attributed to chelation on the amino-group. The $Cu^{2+}$ 2p spectra (Fig. 8) could be observed on KH550-HATP after sorption, while no signals were detected on HATP. Notice the detection depth of XPS is 2–10 nm and the detected element should be on the surface of KH550-HATP. Coupled to the peak displacement of N 1s, it is suggested that Cu ion is adsorbed on amino-group by surface chelation. After the competitive adsorption experiment the Ca 2p peak could not be found, implying that when $Cu^{2+}$ exists, $Ca^{2+}$ is not adsorbed on the surface. This result confirms that the adsorption sites of $Ca^{2+}$ are at least partly different from those of $Cu^{2+}$. To verify this judgment, solo $Cd^{2+}$/$Ca^{2+}$ (26.3 mg $L^{-1}$) adsorption on KH550-HATP was investigated, and XPS patterns of the adsorbed elements were provided. The surface adsorbed $Cd^{2+}$/Si is 0.0092, much less than $Cu^{2+}$/Si (0.0835) and $Ca^{2+}$/Si (0.0829) in the same situation. In summary, it indicates that $Ca^{2+}$ and $Cu^{2+}$ could be chelation adsorbed on amino-group, while the adsorption of $Cd^{2+}$ relies on other mechanisms like internal coordination or static electricity as mentioned, and the chelation priority of $Cu^{2+}$ is higher than that of $Ca^{2+}$. In other words, KH550-HATP has selective chelation adsorption ability to copper ion.

This judgment is also proven by adsorption performance of $Ca^{2+}$, $Cd^{2+}$ and $Cu^{2+}$ on ATP and HATP indirectly (Table S4). The adsorption amount of $Ca^{2+}$ and $Cu^{2+}$ on ATP and HATP is much smaller than that on KH550-HATP, especially

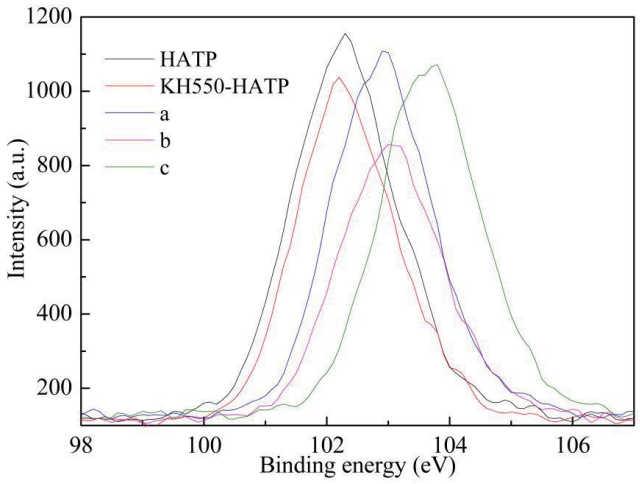


Fig. 6. Si 2p spectra of HATP, KH550-HATP, HATP after copper ion adsorption (a), KH550-HATP after copper ion adsorption (b) and KH550-HATP after competitive adsorption experiment (c).

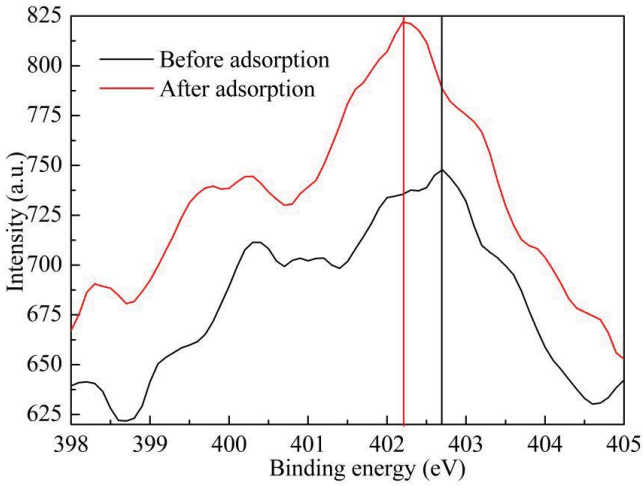


Fig. 7. N 1s spectra of KH550-HATP before and after copper ion adsorption.

relative to the adsorption of $Cd^{2+}$. The adsorption process of copper ions on the surface of KH550 is chelation adsorption (Fig. 3). In addition to providing internal adsorption sites, KH550 also provides the same active adsorption sites as HATP. The copper ions and the amino groups attached to the Si–O and the water in the solution are coordinated and complexed, and then removed.

## 4. Conclusion

Adsorption kinetics study on KH550-HATP with different KH550 contents reveals that copper ion adsorption on high KH550-content materials well follows quasi-second-order kinetics model, and adsorption on low-content materials well follows Elovich model, while the adsorption on both high and low content materials fits quasi-first-order kinetics model. It can be concluded that there are two

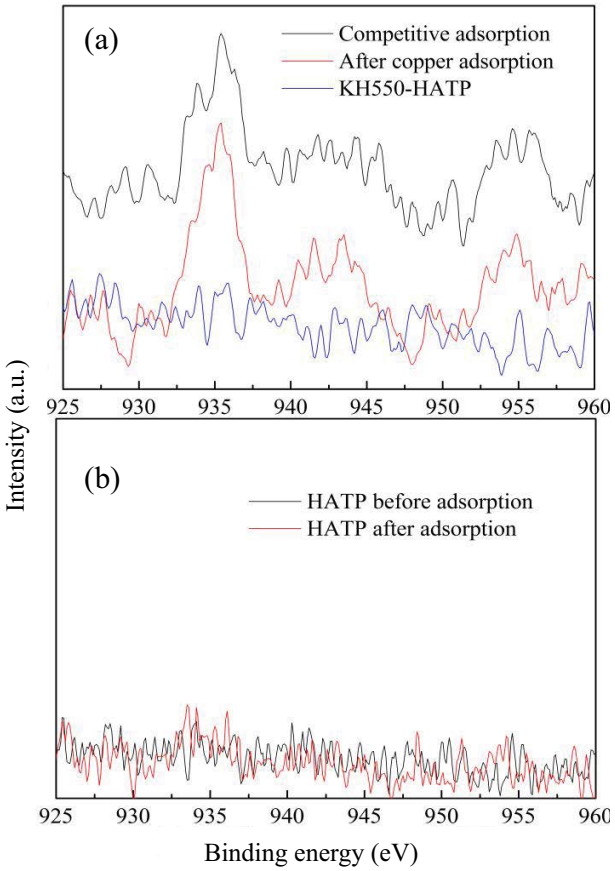


Fig. 8. Cu 2p spectra of KH550-HATP (a) and HATP (b) before and after adsorption.

types of adsorption mechanisms concerning copper ion adsorption on KH550-HATP: interlayer ion exchange and surface chelating. The characterization including XRD, XPS and FTIR directly confirm this judgment. Adsorption isotherms of KH550-HATP at higher temperatures follow Langmuir better than Freundlich equation, whereas at the low temperatures they follow well both the Langmuir and Freundlich equation. It could also imply the dominant position of surface complexation in copper ion adsorption. Competitive experiments indicate that when a high concentration of different ions is involved, only the concentrations of $Cu^{2+}$, $Cd^{2+}$ and $Ca^{2+}$ decrease obviously, and the removal of $Cd^{2+}$/$Ca^{2+}$ from aqueous solution is not primarily caused by inner-sphere complex with amino groups.

## Acknowledgments

This work was supported by the [National Nature Science Foundation of China #1] under Grant [number 21777067]; [the Primary Research & Development Plan of Jiangsu Province #2] under Grant [number BE2019473]; [the Six Talent Peaks Project in Jiangsu Province #3] under Grant [number JNHB105]; [National water pollution control and treatment technology major special subject #4] under Grant [number 2017ZX07202004]; and [the Open Fund of State Environmental Protection Key Laboratory of Wetland Ecology and Vegetation Restoration, Northeast Normal University #5] under Grant [number 130028903] and Introducing Talent Research Start-up Project of Nanjing Normal University.

## References

[1] P. Kjeldsen, M.A. Barlaz, A.P. Rooker, A. Baun, A. Ledin, T.H. Christensen, Present and long-term composition of MSW landfill leachate: a review, Crit. Rev. Env. Sci. Technol., 32 (2002) 297–336.
[2] S.E. Bailey, T.J. Olin, R.M. Bricka, D.D. Adrian, A review of potentially low-cost sorbents for heavy metals, Water Res., 33 (1999) 2469–2479.
[3] J. Rusek, V.G. Marshall, Impacts of airborne pollutants on soil fauna, Annu. Rev. Ecol. Syst., 31 (2000) 395–423.
[4] J. Gans, M. Wolinsky, J. Dunbar, Computational improvements reveal great bacterial diversity and high metal toxicity in soil, Science, 309 (2005) 1387–1390.
[5] Z. Özlem Kocabaş-Atakli, Y. Yürüm, Synthesis and characterization of anatase nanoadsorbent and application in removal of lead, copper and arsenic from water, Chem. Eng. J., 225 (2013) 625–635.
[6] M.R. Awual, I.M.M. Rahman, T. Yaita, M.A. Khaleque, M. Ferdows, pH dependent Cu(II) and Pd(II) ions detection and removal from aqueous media by an efficient mesoporous adsorbent, Chem. Eng. J., 236 (2014) 100–109.
[7] S. Demcak, M. Balintova, M. Demcakova, K. Csach, I. Zinicovscaia, N. Yushin, M. Frontasyeva, Effect of alkaline treatment of wooden sawdust for the removal of heavy metals from aquatic environments, Desal. Water Treat., 155 (2019) 207–215.
[8] U.P. Kiruba, P.S. Kumar, K.S. Gayatri, S.S. Hameed, M. Sindhuja, C. Prabhakaran, Study of adsorption kinetic, mechanism, isotherm, thermodynamic, and design models for Cu(II) ions on sulfuric acid-modified *Eucalyptus* seeds: temperature effect, Desal. Water Treat., 56 (2015) 2948–2965.
[9] T.N. Myasoedova, Y.S. Miroshnichenko, V.A. Gadzhieva, A.I. Chechevatov, M.A. Kremennaya, Y.V. Popov, G.I. Lazorenko, Effective removal of $Pb^{2+}$ and $Cu^{2+}$ from highly concentrated aqueous solutions: comparative sorption study, Desal. Water Treat., 155 (2019) 272–284.
[10] D. Prabu, R. Parthiban, P.S. Kumar, N. Kumari, P. Saikia, Adsorption of copper ions onto nano-scale zero-valent iron impregnated cashew nut shell, Desal. Water Treat., 57 (2016) 6487–6502.
[11] E.K. Putra, R. Pranowo, J. Sunarso, N. Indraswati, S. Ismadji, Performance of activated carbon and bentonite for adsorption of amoxicillin from wastewater: mechanisms, isotherms and kinetics, Water Res., 43 (2009) 2419–2430.
[12] P.-H. Chang, Z.H. Li, T.-L. Yu, S. Munkhbayer, T.-H. Kuo, Y.-C. Hung, J.-S. Jean, K.-H. Lin, Sorptive removal of tetracycline from water by palygorskite, J. Hazard. Mater., 165 (2009) 148–155.
[13] D.G. Kinniburgh, M.L. Jackson, J.K. Syers, Adsorption of alkaline earth, transition, and heavy metal cations by hydrous oxide gels of iron and aluminum, Soil Sci. Soc. Am. J., 40 (1976) 796–799.
[14] X.M. Ma, L. Li, L. Yang, C. Su, K. Wang, S. Yuan, J. Zhou, Adsorption of heavy metal ions using hierarchical $CaCO_3$ maltose meso/macroporous hybrid materials: adsorption isotherms and kinetic studies, J. Hazard. Mater., 209–210 (2012) 467–477.
[15] O. Abollino, M. Aceto, M. Malandrino, C. Sarzanini, E. Mentasti, Adsorption of heavy metals on Na-montmorillonite. Effect of pH and organic substances, Water Res., 37 (2003) 1619–1627.
[16] J. Febrianto, A.N. Kosasih, J. Sunarso, Y.H. Ju, N. Indraswati, S. Ismadji, Equilibrium and kinetic studies in adsorption of heavy metals using biosorbent: a summary of recent studies, J. Hazard. Mater., 162 (2009) 616–645.
[17] R. Celis, M.C. HermosÍn, J. Cornejo, Heavy metal adsorption by functionalized clays, Environ. Sci. Technol., 34 (2000) 4593–4599.

[18] A. Demirbas, Heavy metal adsorption onto agro-based waste materials: a review, J. Hazard. Mater., 157 (2008) 220–229.
[19] C.-Y. Cao, J. Qu, W.-S. Yan, J.-F. Zhu, Z.-Y. Wu, W.-G. Song, Low-cost synthesis of flower like $\alpha$-$Fe_2O_3$ nanostructures for heavy metal ion removal: adsorption property and mechanism, Langmuir, 28 (2012) 4573–4579.
[20] A.M. Liu, K. Hidajat, S. Kawi, D.Y. Zhao, A new class of hybrid mesoporous materials with functionalized organic monolayers for selective adsorption of heavy metal ions, Chem. Commun., 13 (2000) 1145–1146.
[21] A. Shahat, M.R. Awual, M.A. Khaleque, M.Z. Alam, M. Naushad, A.M.S. Chowdhury, Large-pore diameter nano-adsorbent and its application for rapid lead(II) detection and removal from aqueous media, Chem. Eng. J., 273 (2015) 286–295.
[22] M.R. Awual, M.M. Hasan, M.A. Khaleque, M.C. Sheikh, Treatment of copper(II) containing wastewater by a newly developed ligand based facial conjugate materials, Chem. Eng. J., 288 (2016) 368–376.
[23] A. Sari, M. Tuzen, D. Citak, M. Soylak, Adsorption characteristics of Cu(II) and Pb(II) onto expanded perlite from aqueous solution, J. Hazard. Mater., 148 (2007) 387–394.
[24] T. Shi, S. Jia, Y. Chen, Y.H. Wen, C.M. Du, Z.C. Wang, R.L. Qiu, Adsorption characteristics of Cu(II) and Pb(II) ions onto natural manganese ore from aqueous solution, Adsorpt. Sci. Technol., 26 (2008) 613–629.
[25] S. Babel, T.A. Kurniawan, Low-cost adsorbents for heavy metals uptake from contaminated water: a review, J. Hazard. Mater., 97 (2003) 219–243.
[26] H. Chen, A. Wang, Adsorption characteristics of Cu(II) from aqueous solution onto poly(acrylamide)/attapulgite composite, J. Hazard. Mater., 165 (2009) 223–231.
[27] H. Li, R.G. Wang, H.L. Hu, W. Liu, Surface modification of self-healing poly(urea-formaldehyde) microcapsules using silane-coupling agent, Appl. Surf. Sci., 255 (2008) 1894–1900.
[28] P. Liu, Hyperbranched aliphatic polyester grafted attapulgite via a melt polycondensation process, Appl. Clay Sci., 35 (2007) 11–16.
[29] D. Zhao, J. Feng, Q. Huo, N. Melosh, G.H. Fredrickson, B.F. Chmelka, G.D. Stucky, Triblock copolymer synthesis of mesoporous silica with periodic 50 to 300 angstrom pores, Science, 279 (1998) 548–552.
[30] I. Langmuir, The adsorption of gases on plane surfaces of glass, mica and platinum, J. Am. Chem. Soc., 40 (1918) 1361–1403.
[31] T.W. Weber, R.K. Chakravorti, Pore and solid diffusion models for fixed-bed adsorbers, AICHE J., 20 (1974) 228–238.
[32] K.V. Kumar, M.M. de Castro, M. Martinez-Escandell, M. Molina-Sabio, F. Rodriguez-Reinoso, A continuous binding site affinity distribution function from the Freundlich isotherm for the supercritical adsorption of hydrogen on activated carbon, J. Phys. Chem. C, 114 (2010) 13759–13765.
[33] G. Asgari, B. Roshani, G. Ghanizadeh, The investigation of kinetic and isotherm of fluoride adsorption onto functionalize pumice stone, J. Hazard. Mater., 217–218 (2012) 123–132.
[34] J. Wu, M.E. Strömqvist, O. Claesson, I.E. Fängmark, L.G. Hammarström, A systematic approach for modeling the affinity coefficient in the Dubinin–Radushkevich equation, Carbon, 40 (2002) 2587–2596.
[35] M.S. Onyango, Y. Kojima, O. Aoyi, E.C. Bernardo, H. Matsuda, Adsorption equilibrium modeling and solution chemistry dependence of fluoride removal from water by trivalent-cation-exchanged zeolite F-9, J. Colloid Interface Sci., 279 (2004) 341–350.
[36] H. Qiu, L. Lv, B.-c. Pan, Q.-j. Zhang, W.-m. Zhang, Q.-x. Zhang, Critical review in adsorption kinetic models, J. Zhejiang Univ.-Sci. A, 10 (2009) 716–724.
[37] A. Khaled, A.E. Nemr, A. El-Sikaily, O. Abdelwahab, Removal of direct N Blue-106 from artificial textile dye effluent using activated carbon from orange peel: adsorption isotherm and kinetic studies, J. Hazard. Mater., 165 (2009) 100–110.
[38] O.Y. KwonJun, S.W. Choi, Silica-pillared *H*-kenyaites: interlamellar base catalyzed-reaction of tetraethlorthosilicate in water suspension, Bull. Korean Chem. Soc., 20 (1999) 69–75.
[39] H. Chen, Y.G. Zhao, A. Wang, Removal of Cu(II) from aqueous solution by adsorption onto acid-activated palygorskite, J. Hazard. Mater., 149 (2007) 346–354.
[40] J.A. Muller, W.C. Conner, Cyclohexane in ZSM 5.1, FTIR and X-ray studies, J. Phys. Chem., 97 (1993) 1451–1454.
[41] E. Álvarez-Ayuso, A. García-Sánchez, Removal of cadmium from aqueous solutions by palygorskite, J. Hazard. Mater., 147 (2007) 594–600.
[42] Q.H. Fan, X.L. Tan, J.X. Li, X.K. Wang, W.S. Wu, G. Montavon, Sorption of Eu(III) on attapulgite studied by batch, XPS, and EXAFS techniques, Environ. Sci. Technol., 43 (2009) 5776–5782.
[43] D.L. Sparks, Kinetics of Soil Chemical Processes, Academic Press Inc., San Diego, 1989.
[44] Y.S. Ho, Removal of copper ions from aqueous solution by tree fern, Water Res., 37 (2003) 2323–2330.
[45] E. Khademian, E. Salehi, H. Sanaeepur, F. Galiano, A. Figoli, A systematic review on carbohydrate biopolymers for adsorptive remediation of copper ions from aqueous environments-Part A: classification and modification strategies, Sci. Total Environ., 738 (2020) 139829.
[46] C.P. Wang, J.T. Liu, Z.Y. Zhang, B.L. Wang, H.W. Sun, Adsorption of Cd(II), Ni(II), and Zn(II) by tourmaline at acidic conditions: kinetics, thermodynamics, and mechanisms, Ind. Eng. Chem. Res., 51 (2012) 4397–4406.
[47] O.A.C. Monteiro, C. Airoldi, The influence of chitosans with defined degrees of acetylation on the thermodynamic data for copper coordination, J. Colloid Interface Sci., 282 (2005) 32–37.
[48] C.D. Shuang, F. Pan, Q. Zhou, A. Li, P.H. Li, W.B. Yang, Magnetic polyacrylic anion exchange resin: preparation, characterization and adsorption behavior of humic acid, Ind. Eng. Chem. Res., 51 (2012) 4380–4387.
[49] Y.T. Zhou, C. Branford-White, H.L. Nie, L.M. Zhu, Adsorption mechanism of $Cu^{2+}$ from aqueous solution by chitosan-coated magnetic nanoparticles modified with $\alpha$-ketoglutaric acid, Colloid. Surf., B, 74 (2009) 244–252.
[50] B.J. Gao, Y.C. Gao, Y.B. Li, Preparation and chelation adsorption property of composite chelating material poly(amidoxime)/$SiO_2$ towards heavy metal ions, Chem. Eng. J., 158 (2010) 542–549.
[51] H.-J. Im, Y. Yang, L.R. Allain, C.E. Barnes, S. Dai, Z.L. Xue, Funtionalized sol-gels for selective copper(II) separation, Environ. Sci. Technol., 34 (2000) 2209–2214.

**Supplementary information**

Table S1
Concentration (mg $L^{-1}$) of the metal ion in the tests for the investigation of the effect of different ionic strength (sorbent concentration = 1.5 g $L^{-1}$)

| | $Na^+$ | $Mg^{2+}$ | $K^+$ | $Ca^{2+}$ | $Ni^{2+}$ | $Cd^{2+}$ | $Co^{2+}$ | $Cu^{2+}$ |
|---|---|---|---|---|---|---|---|---|
| Separated solution | 9.8 | 3.0 | 13.1 | 9.0 | 5.0 | 9.1 | 5.1 | 6.6 |
| Mixed solution 1 (*M*1) | 9.8 | 3.0 | 13.1 | 9.0 | 5.0 | 9.1 | 5.1 | 6.6 |
| Mixed solution 2 (*M*2) | 19.7 | 6.0 | 26.2 | 18.1 | 10.1 | 18.2 | 10.1 | 13.2 |
| Mixed solution 3 (*M*3) | 39.3 | 12.0 | 52.4 | 36.1 | 20.2 | 36.4 | 20.2 | 26.3 |
| Mixed solution 4 (*M*4)[a] | 26.3 | 26.3 | 26.3 | 26.3 | 26.3 | 26.3 | 26.3 | 26.3 |

[a]This set was for desorption experiment and XPS characterization.

Table S2
The quasi-first-order and quasi-second-order kinetics fitting constants of $Cu^{2+}$ adsorption by KH550-HATP with different KH550 contents

| KH550 contents | Quasi-first-order kinetics constants[a] | | | Quasi-second-order kinetics constants | | |
|---|---|---|---|---|---|---|
| | $C_{e1}$ (mg $L^{-1}$) | $k_1$ ($min^{-1}$) | $R^2$ | $C_{e2}$ (mg $L^{-1}$) | $k_2$ (g $mg^{-1}$ $min^{-1}$) | $R^2$ |
| K100/100 | 0.0574 | 0.0662 | 0.9894 | 0.0574 | 0.0452 | 0.973 |
| K100/20 | 0.0515 | 0.0362 | 0.973 | 0.0515 | 0.0332 | 0.953 |
| K100/10 | 0.0684 | 0.0713 | 0.977 | 0.0683 | 0.0525 | 0.8785 |
| K100/5 | 0.0689 | 0.0204 | 0.938 | 0.0689 | 0.0177 | 0.8783 |
| K100/8 | 0.053 | 0.0246 | 0.9698 | 0.054 | 0.0147 | 0.9612 |
| | Elovich constants | | | Intraparticle diffusion constants[b] | | |
| | $\alpha$ (mg $g^{-1}$ $min^{-1}$) | β (g $mg^{-1}$) | $R^2$ | $k_3$ (mg $g^{-1}$ $min^{-1/2}$) | $C$ (mg $g^{-1}$) | $R^2$ |
| K100/100 | 3,730.98 | 3.35 | 0.7823 | 0.2248 | 2.6194 | 0.9403 |
| K100/20 | 159.18 | 2.61 | 0.8959 | 0.2377 | 2.3102 | 0.9962 |
| K100/10 | 48,113.81 | 3.97 | 0.6359 | 0.198 | 2.8628 | 0.7213 |
| K100/5 | 5.80 | 1.88 | 0.9919 | 0.2232 | 1.8013 | 0.9765 |
| K100/8 | 9.37 | 1.92 | 0.923 | 0.2897 | 1.5713 | 0.9843 |
| | $R^2$ of $B_t$ vs. $t$ plot | | | | | |
| K100/100 | 0.997 | | | | | |
| K100/20 | 0.9976 | | | | | |
| K100/10 | 0.9898 | | | | | |
| K100/5 | 0.9491 | | | | | |
| K100/8 | 0.9597 | | | | | |

[a]The quasi-first-order kinetics fitting and $B_t$ vs. $t$ plot for K100/100 and K100/10 included only 0–180 min.
[b]Intraparticle diffusion kinetics fitting included only 10–60 min.

Table S3
Langmuir, Freundlich, Temkin and Dubinin–Radushkevich isotherm constants of $Cu^{2+}$ adsorption by KH550-HATP at different temperatures

| Temperature (K) | Langmuir constants | | | | Freundlich constants | | |
|---|---|---|---|---|---|---|---|
| | $b$ (L mg$^{-1}$) | $q_{max}$ (mg g$^{-1}$) | $R^2$ | $R_L$ ($C_0$ = 26.3 mg L$^{-1}$) | $K_F$ (mg g$^{-1}$) | $n$ | $R^2$ |
| 283 | 0.2875 | 3.33 | 0.9872 | 0.1168 | 1.6289 | 6.1387 | 0.8958 |
| 293 | 0.573 | 5.92 | 0.9968 | 0.0622 | 2.6506 | 4.2644 | 0.9119 |
| 303 | 12.2143 | 9.75 | 0.9957 | 0.0031 | 4.9303 | 3.7133 | 0.8565 |
| 313 | 9.5 | 13.85 | 0.9951 | 0.004 | 7.8507 | 3.864 | 0.6253 |
| Temperature (K) | Temkin constants | | | Dubinin–Radushkevich constants | | | |
| | $k_t$ (L mg$^{-1}$) | $B_t$ (kJ mol$^{-1}$) | $R^2$ | $q_D$ (mg g$^{-1}$) | $B_D$ (× 10$^{-3}$ mol$^2$ kJ$^{-2}$) | $R^2$ | $E_a$ (kJ mol$^{-1}$) |
| 283 | 57.873 | 6.177 | 0.851 | 4.6654 | 1.6 | 0.8633 | 17.68 |
| 293 | 22.651 | 2.789 | 0.8931 | 11.8552 | 2.1 | 0.9221 | 15.43 |
| 303 | 45.145 | 1.638 | 0.8414 | 26.3578 | 2.1 | 0.903 | 15.43 |
| 313 | 124.959 | 1.319 | 0.7278 | 40.361 | 1.9 | 0.6845 | 16.22 |

Table S4
Competitive adsorption experiment of HATP in a mixture of $Ca^{2+}$, $Cd^{2+}$ and $Cu^{2+}$

| Concentration (mg L$^{-1}$) | Ca | Cd | Cu |
|---|---|---|---|
| Initial concentration | 28.9 | 28.8 | 29.1 |
| Rest concentration for ATP | 38.2 | 16.8 | 22.2 |
| Rest concentration for HATP | 25.9 | 17.9 | 25.3 |

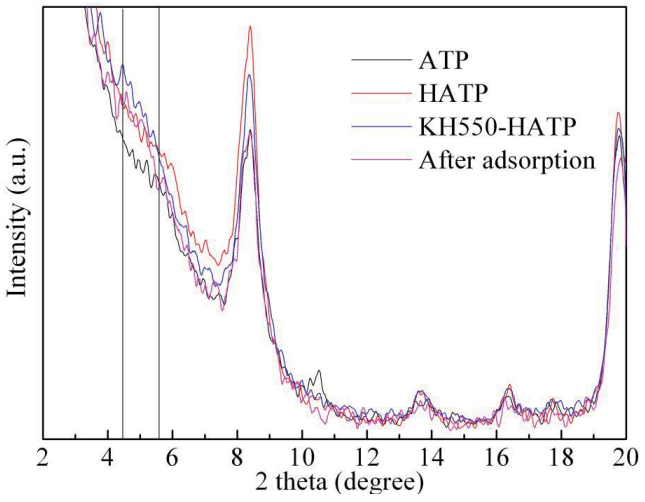


Fig. S1. XRD patterns of ATP, HATP, KH550-HATP and KH550-HATP after copper ion adsorption.

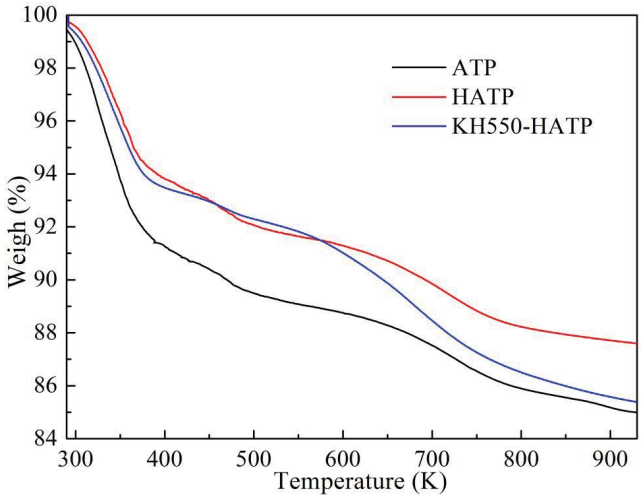


Fig. S2. TGA data of ATP, HATP and KH550-HATP (in air).

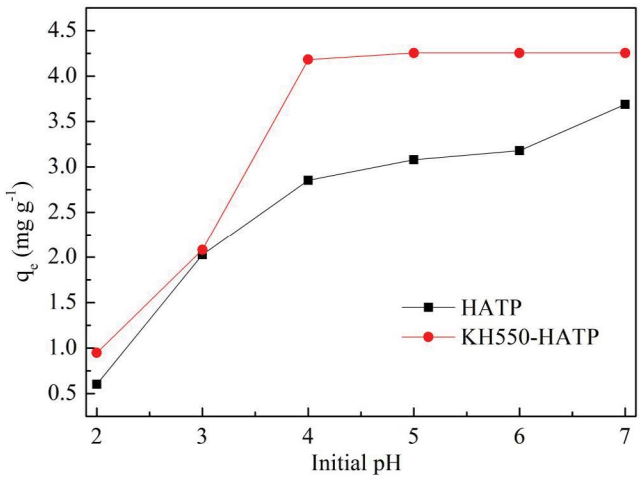


Fig. S3. Effect of initial pH on $Cu^{2+}$ adsorption on HATP and KH550-HATP.

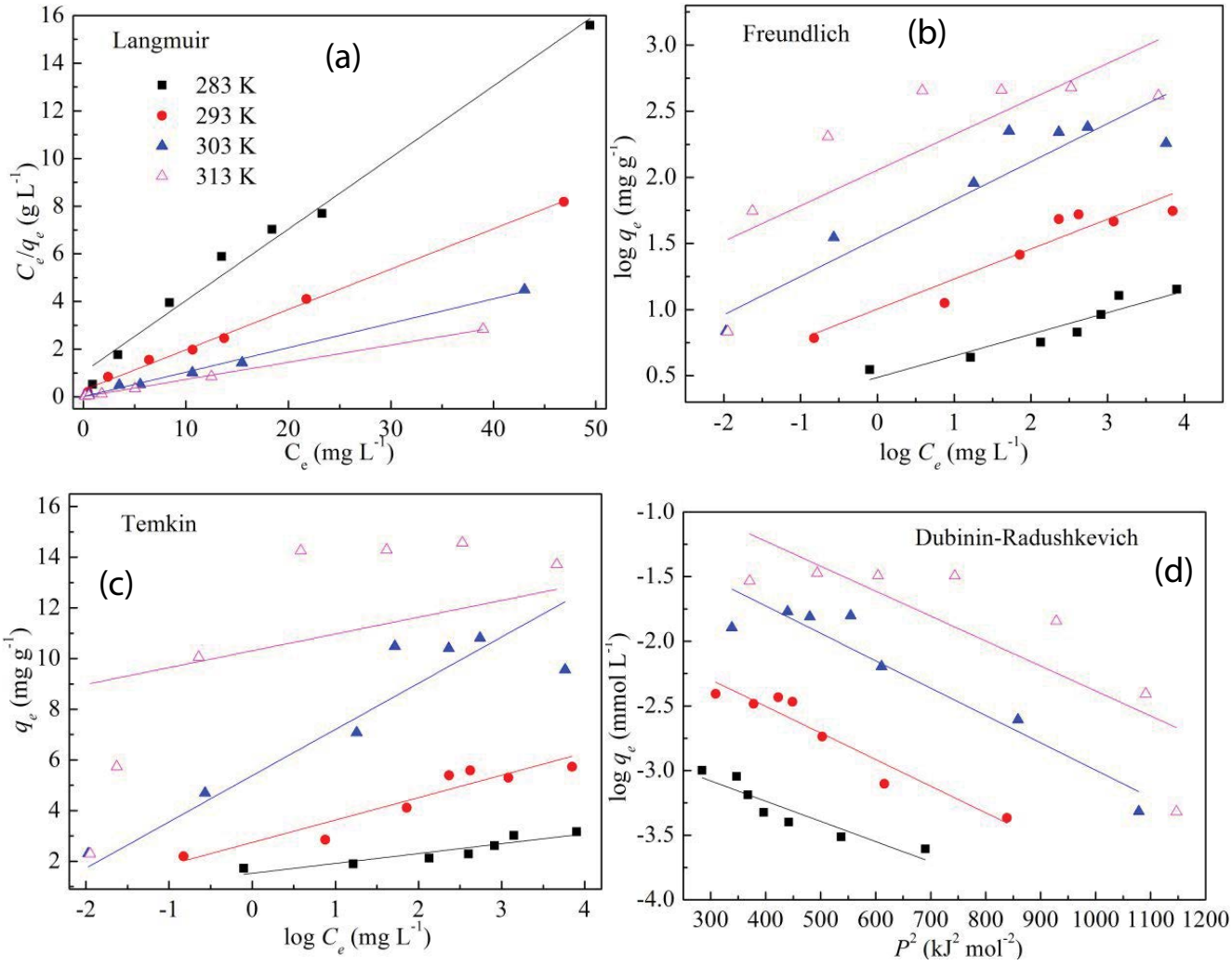


Fig. S4. (a) Langmuir, (b) Freundlich, (c) Temkin and (d) Dubinin–Radushkevich plots for the adsorption of Cu(II) onto KH550-HATP at different temperatures.